




Effect of crystallization and packing pressure on the development of residual stresses on injection molded polypropylene samples

M. Estrella-Guayasamin¹ · U. Figueroa-López¹ · A. Guevara-Morales¹ · R. A. García-León² 

Received: 9 February 2022 / Revised: 6 April 2022 / Accepted: 3 May 2022 /
Published online: 23 May 2022

© The Author(s), under exclusive licence to Springer-Verlag GmbH Germany, part of Springer Nature 2022

Abstract

Thermoplastics processing usually involves the non-uniform cooling of molten polymer, which results in the presence of residual stresses in the final product. The magnitude of these stresses can be high enough to induce severe shape changes in the product, as well as changes in the overall material performance. Because of this, it is important to be able to accurately predict and measure them. In this study, the effect of coupling a kinetic model of crystallization on the prediction of thermal and pressure-induced residual stresses using the residual temperature field and formation pressure concepts is investigated. In addition, the effect of packing pressure on the deflection of injection molded polymer plates after ejection is reported. Simulation results were compared with experimental data, and it was found that considering crystallization in the prediction of residual stresses decreased the % error between predicted deflection and experimental results, from 0.52–7.34 to 3.0–56.3%. Also, good agreement between experimental results and the simulations performed using the residual temperature and pressure fields concepts in 2D while including a kinetic model of crystallization with different packing pressures.

Keywords Crystallization · Residual stresses · Simulation · Packing pressures

✉ U. Figueroa-López
ufiguero@tec.mx

✉ A. Guevara-Morales
a.guevaram@tec.mx

✉ R. A. García-León
ragarcial@ufps.edu.co

¹ Escuela de Ingeniería y Ciencias, Tecnológico de Monterrey, Carretera Lago de Guadalupe km. 3.5, CP. 52926 Atizapan de Zaragoza, México

² Facultad de Ingenierías. Grupo de Investigación INGAP, Universidad Francisco de Paula Santander Ocaña, CP. 546552 Ocaña, Norte de Santander, Colombia

Introduction

During the thermoplastics processing, non-uniform cooling generates residual stresses over the polymer samples. Thermal stresses appear during cooling. In injection molded products, for example, material in contact with the mold walls is cooled faster than the material at the core and, as the material cools down, strains are developed in the solid phase due to the constraint in the contraction induced by crystallization. These frozen-in strains give rise to stresses through the modulus of the solid material. Pressure-induced residual stresses, on the other hand, are built up and locked in the material due to the high pressures applied during the filling and packing stages of the injection molding process. The magnitude of these stresses can be high enough to induce severe shape changes in the product.

In addition to the shape distortion, the presence of residual stresses is also expected to affect the mechanical behavior of the product such as impact strength [1], crack propagation [2] and fatigue life [3], among others. Because of this, it is important to be able to accurately predict and measure them. Although several models and simulations [4–7] have been developed over the years to predict flow, pressure and thermal-induced residual stresses in injection molded products, investigating the effect of crystallinity evolution on the generation of residual stresses in injection molded plastic parts is still required.

Kamal et al. [8] developed a linear elastic and linear thermoviscoelastic compressible model to predict thermal-induced residual stresses, applied to thin wall injection molded parts, considering crystallization effects. Jansen et al. [9, 10] presented a thermoelastic model to predict thermal-induced residual stresses assuming a simple elastic behavior for the solid, including effects of crystallization and external forces. In both approaches, the effect of crystallization was considered through the densification process of the polymer due to the tighter packing of the crystalline phase compared to the amorphous one. This densification process will lead to anisotropy and other changes in mechanical properties such as elastic modulus, yield strength, ultimate strength and thermal properties such as the thermal expansion coefficient [4] and the glass transition temperature [8]. However, the evolution of latent heat during crystallization [11] will also affect the thermal history of the polymer melt during the different stages of injection molding, mainly packing and cooling, and thus the generation and distribution of residual stresses.

In this study, the effect of including a kinetic model of crystallization developed by Phillips and Manson [12] to predict the evolution of the absolute crystallinity within the polymer plate during the injection molding process on the prediction of thermal and pressure-induced residual stresses is analyzed. For this, 2D simulations using the residual temperature field [13, 14] and pressure formation [15] concepts are performed with and without the kinetic model of crystallization and results are compared with experimental results. In addition, the effect of packing pressure on the distribution of residual stresses is also analyzed in simulations including the kinetic model of crystallization.

Materials and methods

Material

The material used in this study was a polypropylene copolymer (Formolene 2610A), without filler, widely used in automotive applications due to its ease to mold, good impact resistance and good dimensional stability. Its mechanical, physical and thermal properties are summarized in Table 1. Note that thermal conductivity and specific heat are thermal dependent properties that were coupled in the simulations through piecewise equations in the User Defined Material Database.

The rheological behavior of the material was modeled as a generalized Newtonian fluid through the modified cross-WLF model using Eq. 1:

$$\eta(T, \dot{\gamma}, p) = \frac{\eta_0(T, p)}{1 + \left(\frac{\eta_0(T, p)\dot{\gamma}}{\tau^*}\right)^{1-n}} \tag{1}$$

where η is the melt viscosity (Pa-s), $\dot{\gamma}$ is the shear rate (1/s), τ^* is the critical stress level at the transition to shear thinning (Pa), n a power law exponent and η_0 is the zero-shear viscosity (Pa-s) defined as Eq. 2:

$$\eta_0(T, p) = D_1 \exp \left[\frac{-A_1(T - T^*)}{A_2 + (T - T^*)} \right] \tag{2}$$

where T is the temperature (K), T^* is a reference temperature determined by curve fitting ($T^* = D_2 + D_3p$), p is the pressure (Pa), $A_2 = A_3 + D_3p$ and A_1, A_3, D_1, D_2 and D_3 are data-fitted coefficients. From [16], the following coefficients were used: $\tau^* = 31,672.05$, $n = 0.29$, $A_1 = 21.48$, $A_3 = 0.49$, $D_1 = 2.38 \times 10^{12}$, $D_3 = 0$ and $T^* = D_2 = 191.08$.

Table 1 Mechanical, physical and thermal properties of polypropylene copolymer formolene 2610A

Property	Symbol	Unit	Value	Source
Density	ρ	kg/m ³	900	Datasheet
Specific heat	$C_p(T)$	J/kg K	1800–3600	[16]
Thermal conductivity	$k(T)$	W/m K	0.131–0.241	[17]
Latent heat of fusion	H_c	kJ/kg	209	[12]
Melting temperature	T_m	°C	127.12	[16]
Thermal expansion coefficient	α	1/°C	0.00016	[11]
Long term modulus	E_∞	MPa	643	[16]
Young modulus	E	MPa	1175.8	[16]

Numerical analysis

Numerical analysis was performed in three stages using ANSYS Workbench R18.1 and MATLAB R18b: (1) obtaining the pressure and temperature fields, (2) estimating residual stresses, and (3) predicting the deformation of the molded plate.

Pressure and temperature fields

Constitutive equations The temperature and pressure histories of the polymer during the three stages of the injection molding process are needed to estimate the thermal and pressure induced residual stresses in an injection molded product. For this, the constitutive equations of momentum (Eq. 3), mass (Eq. 5) and energy (Eq. 6) are solved using a CFD software.

Conservation of momentum:

$$\frac{\partial}{\partial t}(\rho\vec{v}) + \nabla \cdot (\rho\vec{v}\vec{v}) = \nabla p + \nabla \cdot (\vec{\bar{\tau}}) + \rho\vec{g} + \vec{F} \quad (3)$$

$$\text{where : } \vec{\bar{\tau}} = \eta[(\nabla\vec{v} + \nabla\vec{v}^T) - \frac{2}{3}\nabla \cdot \vec{v}I] \quad (4)$$

Conservation of mass:

$$\frac{\partial \rho}{\partial t} + \nabla \cdot (\rho\vec{v}) = 0 \quad (5)$$

Conservation of energy:

$$\frac{\partial}{\partial t}(\rho U) + \nabla \cdot (\vec{v}(\rho U + p)) = \nabla \cdot \left(k\nabla T + \left(\vec{\bar{\tau}} \cdot \vec{v} \right) \right) + \rho H_c \frac{\partial X_c}{\partial t} \quad (6)$$

Considering that ρ is the density, \vec{v} is the fluid velocity, p the static pressure, $\vec{\bar{\tau}}$ the extra-stress tensor, \vec{g} the gravitational force, \vec{F} the external body forces, η the viscosity as defined by Eq. 1, T the temperature, k the thermal conductivity, U the energy defined as $U = h - \frac{p}{\rho} + \frac{v^2}{2}$, h the enthalpy, H_c the latent heat of fusion and X_c the fraction of crystallized material.

Crystallization ΔX_c was calculated using a kinetic model proposed by Phillips and Manson [12], based on the modifications and assumptions proposed by [18, 19]. Relative crystallinity at time t , $v_c(t)$, considering spherulite impingement and nonisothermal crystallization, is described as:

$$\frac{v_c(t)}{1 - v_c(t)} = \int_0^t \kappa(T) m t^{m-1} dt \quad (7)$$

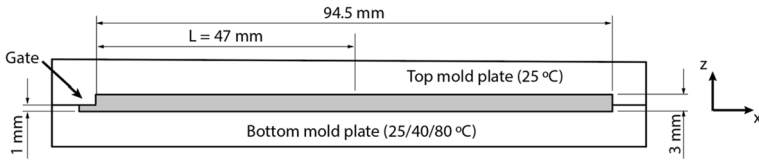


Fig. 1 Simplified 2D model of a rectangular plate for the injection-molding simulation

where κ is the rate constant. m the Avrami exponent and T the temperature. Using an Avrami exponent $m=4$ for homogeneous nucleation and $m=3$ for heterogeneous nucleation. Eq. 7 can be rewritten as

$$\varphi = \frac{v_c(t)}{1 - v_c(t)} = \int_0^t 3\kappa_{het}(T(\psi))\psi^2 d\psi + \frac{\varepsilon \int_0^t 4\kappa_{hom}(T(\psi))\psi^3 d\psi}{1 + (1 - \varepsilon) \int_0^t 4\kappa_{hom}(T(\psi))\psi^3 d\psi} \quad (8)$$

where: $\varepsilon = \frac{X_{c,\infty,hom}}{X_{c,\infty,het}}$, which accounts for the fact that heterogeneous nucleation is dominant at low cooling rates and homogeneous nucleation is dominant at high cooling rates and therefore, the absolute crystallinity at equilibrium under heterogeneous nucleation $X_{c,\infty,het}$ is higher than that under homogeneous nucleation, $X_{c,\infty,hom}$. Finally, absolute crystallinity is defined as:

$$X_c(t) = X_{c,\infty,het} \left(\frac{\varphi}{1 + \varphi} \right) \quad (9)$$

If the absolute crystallinity X_c is obtained at every time step of the heat transfer analysis, the fraction of crystallized material ΔX_c can be found. Note that for the nonisothermal case the rate constants, κ_i , are expressed as a function of temperature. They are defined as Eqs. 10 and 11:

$$\kappa_{het} = C_{11} \exp \left[- \left(\frac{C_{12}}{T(T_m^0 - T)^2} + \frac{C_{13}}{T - T_g + 51.6} \right) \right] \quad (10)$$

$$\kappa_{hom} = C_{21} \exp \left[- \left(\frac{C_{22}}{T(T_m^0 - T)^2} + \frac{C_{23}}{T - T_g + 51.6} \right) \right] \quad (11)$$

where T_m^0 is the equilibrium melting temperature, T_g is the glass transition temperature and the constants C_{ij} are functions of physical constants. In this study, the constants reported by Phillips [12] for a PP with similar properties to PP-Co 2016 were used: $C_{11} = 1.41 \times 10^{28} s^{-3}$, $C_{12} = 3.94 \times 10^7 K^3$, $C_{13} = 10,790K$, $C_{21} = 4.64 \times 10^{18} s^{-4} K^{-1}$, $C_{22} = 9.56 \times 10^7 K^3$ and $C_{23} = 4396K$. $T_m^0 = 185 \text{ }^\circ\text{C}$, $T_g = -10 \text{ }^\circ\text{C}$, $X_{c,\infty,hom} = 0.43$ and $X_{c,\infty,het} = 0.52$.

Geometry The injection molding process of a rectangular plate of $94.5 \times 55.0 \times 3.0$ mm was simulated in ANSYS Fluent 18.1 using a simplified 2D model as shown in Fig. 1.

An adaptive quadrilateral-dominant mesh with an average size of 0.1 mm was used with a refined region of 0.02 mm near the walls. A pressure-implicit with splitting of operators (PISO) pressure–velocity coupling scheme was implemented along an implicit volume of fluid (VOF) multiphase model.

Boundary conditions For the boundary conditions were considered the following assumptions:

- Inlet boundary: a 1 mm thick rectangular gate was used to fill the mold cavity with an injection pressure $P_{\text{injection}} = 4$ MPa, and a packing pressure P_{packing} equal to 3.2, 4.0 or 4.8 MPa depending on the packing conditions (80, 100 or 120% of the injection pressure). The transition from injection to packing pressure (switch-over) was defined at 0.67 s, when the mold is almost full (95%). Packing pressure was held until the gate froze, at which time cooling starts and pressure was set to 0.05 MPa.
- Outlet boundary: three vents at the corners of the mold allow the release of air during the filling stage with $P_{\text{outlet}} = P_{\text{atm}} = 101.3$ kPa and $T_{\text{outlet}} = 25$ °C.
- Mold temperature at top plate $T_{\text{top}} = 25$ °C, and mold temperature at bottom plate T_{bot} equal to 25, 40 or 80 °C depending on the cooling case (symmetrical or asymmetrical cooling conditions). Note that although the recommended surface mold temperatures for PP are between 15 and 50 °C, the 80 °C mold temperature provided good quality injection molded samples with a more severe temperature gradient that was considered useful for this study.

Residual stresses calculation

In this study, flow-induced residual stresses are neglected as it has been widely reported [5, 20] that they are significantly lower thermal and pressure-induced stresses. To calculate thermal-induced residual stresses, temperature gradients at the moment of solidification are integrated to obtain the residual temperature field, T_{res} , as defined by Tropsha et al. [13] The residual stress distribution $\sigma_{\text{res}}(z)$ in a viscoelastic plate is then calculated using Eq. 12:

$$\sigma_{\text{res}}(z) = \frac{E_{\infty}}{1 - \nu} \alpha \left[\bar{T}_{\text{res}} - T_{\text{res}}(z) \right] \quad (12)$$

where \bar{T}_{res} is the average value of T_{res} through the thickness of the plate, E_{∞} is the long-term modulus of the material, α is the coefficient of thermal expansion and ν is the Poisson modulus of the material equal to 0.33.

In a similar way, the residual pressure-induced stresses were calculated using Eq. 13 [15]:

$$\sigma_{\text{pres}}(z) = -\frac{1 - 2\nu}{1 - \nu} \left[P_f(z) - \bar{P}_f \right] \quad (13)$$

where the formation pressure P_f is the pressure at the time of solidification at each computational point and \bar{P}_f is the average value of P_f through the thickness of the plate.

Prediction of plate deflection

To obtain the plate deflection, the total residual stress distribution (thermal- and pressure-induced) was imported into a 2D ANSYS Mechanical Structural model. A distance-based average mesh mapping with eight interpolation points was used to transfer data from one mesh to another (from Fluent to Mechanical Structural). QUAD4 elements with a size of 0.2 mm were used. Simply supported conditions were defined at the bottom corners of the plate.

Experimental analysis

Injection molding

A 50-ton Belken/SSF500-K5 injection molding machine coupled with pressure and temperature Kistler/6190CA sensors was used. To reach the desired mold temperature, a hydronic heating system was used, in which a PEAK anti-freeze + coolant solution was heated in a deposit and pumped through a distribution system through the mold. This distribution system consisted of two circular channels of 9 mm of diameter, aligned parallel to the plate length and positioned 10 mm beneath the mold surface. This heating system provided us a variation of ± 3 °C from the desired mold surface temperature. Once ejected, a 10 mm wide strip was cut from the mid-section of each plate (Fig. 2a). Once the strips were cut, they were kept at room temperature for 48 h, allowing stress relaxation as reported in [16].

Plate deflection measurement

Deflection was estimated through the curvature measurements on the 10 mm wide strips. Curvatures were measured using the digital image processing module in MATLAB, in which 1200 dpi resolution images of the deflected strips obtained with a HP deskjet ink advantage were imported (Fig. 2b). The edge detection tool with a Laplacian of Gaussian (LoG) filter was used to select 50 different points along the curvature (Fig. 2c) which were then fitted to a circumference of radius R using least-squares. Maximum deflection was estimated through the height of the arc.

Results and discussion

Effect of crystallization on residual stresses and plate deflection

With the aim of analyzing the effect of crystallization on the residual stress generation, simulations were run according to the previous sections with and without the crystallization module coupled. This is, ΔX_c was either defined as zero (no crystallization) or obtained as described in [Crystallization](#) section.

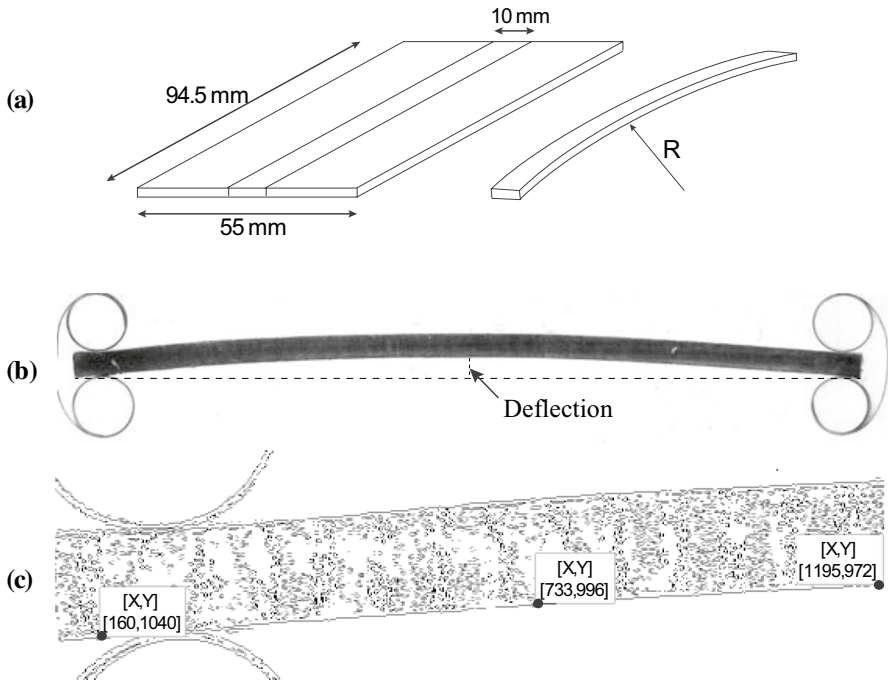


Fig. 2 **a** 10 mm wide strip for curvature measurements cut from molded plate, **b** scanned image of deflected strip and **c** edge detection tool used to obtain 50 points along the curvature

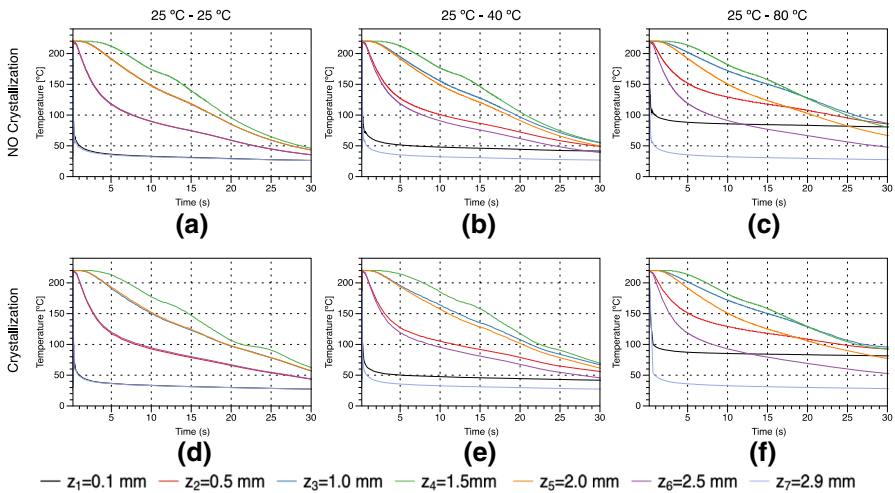


Fig. 3 Thermal histories of polymer melt without considering the crystallization model for **a** 25–25 °C, **b** 25–40 °C and **c** 25–80 °C cooling cases; and considering the crystallization model for **d** 25–25 °C, **e** 25–40 °C and **f** 25–80 °C cooling cases

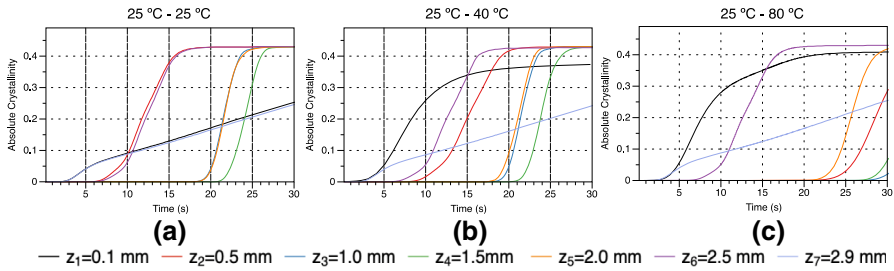


Fig. 4 Crystallinity evolution of the polymer across the thickness of the plate for different cooling conditions: **a** 25–25 °C, **b** 25–40 °C and **c** 25–80 °C

In Fig. 3, thermal histories of the polymer melt across the thickness of the plate at a length $L = 47$ mm (see Fig. 1), for the symmetrical and asymmetrical cooling conditions, with and without the crystallization model coupled, are shown. As expected, for the symmetrical cooling conditions, the cooling rate for the top and bottom layers is almost the same (a small difference is observed, which is attributed to the location of the gate at the bottom plate), with a very high thermal gradient due to the contact of the polymer melt with the cold mold (almost an instant solidification). For the middle or core layers, the cooling rate is much slower. A similar behavior in cooling rates is observed for the asymmetrical cooling cases, fast at the surface, slow at the core. However, in these cases the bottom surface (at 40 or 80 °C) solidifies slightly after the top one. Now, the effect of crystallization is better observed at the core layers ($z_4 = 1.5$ mm) where a plateau in temperature is observed due to the evolution of latent heat (heat source on the balance equation) [11]. Note that although differences in the thermal histories is more evident for the slowly cooled regions, it does affect the thermal history of the entire molded part.

The appearance of this temperature plateau at time $t \approx 20$ s, $t \approx 21$ s, and $t \approx 27$ s for the 25–25 °C, 25–40 °C, and 25–80 °C cooling cases, respectively, agrees well with the evolution of absolute crystallinity shown in Fig. 4. Note that for the 25–25 °C and 25–40 °C cases, crystallization at the core layer ($z_4 = 1.5$ mm) starts at $t \approx 20$ s, while for the 25–80 °C cooling case, it seems to start after 25 s. Note that for the purpose of this study, in which residual stresses are built up upon solidification, the simulations are stopped after 30 s, when all the layers have reached temperatures below 100 °C, so the crystallinity levels shown at 30 s do not represent the final degree of crystallinity of the molded part.

Because flow-induced residual stresses are neglected in this study, residual stresses in the injection molded product will be given by the sum of thermal- and pressure-induced stresses. In Fig. 5 the obtained thermal, pressure, and total-stress distribution are shown for simulations with and without crystallization. The results for top ($z = 3$ mm), middle ($z = 1.5$ mm) and bottom ($z = 0$ mm) positions are summarized in Table 2.

The total residual stress distribution for both simulations, with and without crystallization, presents compressive stresses at the surfaces and tensile at the core

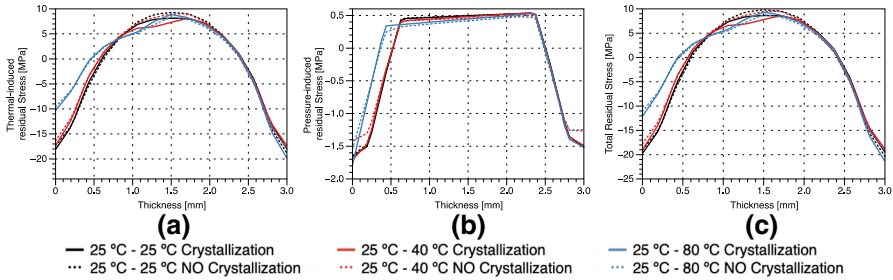


Fig. 5 **a** Thermal, **b** pressure and **c** total residual stresses at polymer plates cooled under different conditions with and without considering a kinetic model of crystallization

(Fig. 5c). Although the distribution is similar, the magnitude of the stresses is different while considering or not crystallization. For symmetrical cooling, the maximum compressive stresses in the top and bottom layers without considering crystallization vary $\sim \pm 4\%$ in comparison to those obtained with the crystallization module. However, in the core layers, maximum tensile stresses up to $\sim 13\%$ higher were found when crystallization was not considered. Something similar occurs for the asymmetrical cooling conditions, 25–40 °C and 25–80 °C, in which variations of approximately 2 and -10% in the compressive stresses of top layers; -7 and -8% in the compressive stresses of bottom layers; and 21 – 6% in the tensile stresses at the core layers were found. Note that it is in the middle layers where the effect of considering or not the crystallization model has a more significant effect. For the 25–25 °C and 25–40 °C cases, tensile stresses at the core decreased with crystallization, which might be explained by the lower temperature gradients at the core layer that decreased the overall stress distribution. For the 25–80 °C case, crystallization at the core layer starts after ~ 25 s, while at the surfaces it starts much earlier, generating higher temperature gradients and thus increasing residual stresses.

In Table 3, computed maximum deflection of the plates for the symmetrical (25–25 °C) and asymmetrical (25–40 °C and 25–80 °C) cooling conditions with and without considering crystallization are reported. The experimental results are also shown for comparison. As expected, simulation results when crystallization is considered are closer to the experimental results than those where crystallization was not accounted for. Errors up to 56.37% were found when crystallization is not included in the simulations. For the 25–25 °C and 25–40 °C cases, deflection is lower when crystallization is not considered. On the other hand, for the 25–80 °C case, deflection without considering crystallinity slightly increases. This is in agreement with the reported values of stresses from Table 2.

Effect of packing pressure on residual stresses and plate deflection

With the aim of analyzing the effect of the packing pressure on the residual stress distribution and the deformation of the plate, new simulations were performed varying the packing pressure from 80, 100 and 120% of the injection pressure. For this, two cases were studied: symmetrical (25–25 °C) and asymmetrical

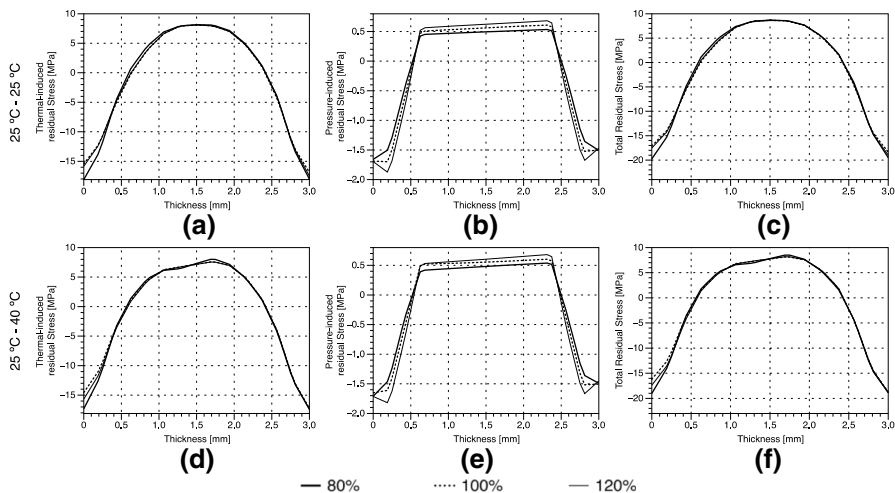
Table 2 Thermal, pressure and total residual stresses at the top, middle and bottom layers of an injection molded polymer plate under different cooling conditions with and without considering crystallization

	25 °C-25 °C			25 °C-40 °C			25 °C-80°C		
	Cryst.	No. Cryst.	% dif.	Cryst.	No. Cryst.	% dif.	Cryst.	No. Cryst.	% dif.
Thermal-induced residual stresses (MPa)									
Top	-18.00	-18.85	4.73	-17.38	-18.02	3.67	-19.86	-17.92	-9.76
Middle	8.14	9.30	14.25	-7.32	8.99	22.80	8.88	8.84	-0.51
Bottom	-18.09	-19.02	5.10	-17.32	-16.37	-5.46	-10.34	-9.59	-7.24
Pressure-induced residual stresses (MPa)									
Top	-1.51	-1.51	0.40	-1.42	-1.27	-10.78	-1.52	-1.24	-17.94
Middle	0.49	0.50	0.61	0.48	0.46	-5.19	0.45	0.42	-6.28
Bottom	-1.66	-1.65	-0.84	-1.71	-1.41	-17.43	-1.78	-1.54	-13.62
Total residual stresses (MPa)									
Top	-19.51	-20.37	4.39	-18.87	-19.28	2.19	-21.37	-19.16	-10.33
Middle	8.64	9.80	13.45	7.80	9.45	21.07	9.33	8.80	-5.67
Bottom	-19.75	-19.02	-3.73	-19.03	-17.78	-6.56	-12.12	-11.13	-8.18

Top ($z=3$ mm), middle ($z=1.5$ mm) and bottom ($z=0$ mm).

Table 3 Maximum deflection of the plates obtained through experimental measurements and simulations with and without considering crystallization

	25–25 °C	25–40 °C	25–80 °C
Experimental [mm]	0.32	0.61	2.22
Simulation–crystallization [mm]	0.32	0.57	2.07
Simulation–NO crystallization [mm]	0.18	0.26	2.15
% error–rystallization	0.52	7.29	7.34
% error–NO crystallization	43.91	56.37	3.0

**Fig. 6** a–d Thermal, b–e pressure and c–f total residual stresses at polymer plates cooled under different conditions and packing pressures**Table 4** Thermal, pressure and total residual stresses at the top, middle and bottom layers of an injection molded polymer plate under different packing conditions

		25–25 °C			25–40 °C		
		80%	100%	120%	80%	100%	120%
Thermal-induced residual stresses (MPa)	Top	–18	16.85	–17.49	–17.38	–17.24	–17.4
	Middle	8.14	8.09	8.09	7.32	7.19	7.18
	Bottom	–18.09	–15.43	–15.84	–17.32	–14.54	–15.67
Pressure-induced residual stresses (MPa)	Top	–1.51	–1.5	–1.47	–1.49	–1.51	–1.45
	Middle	0.49	0.56	0.62	0.48	0.55	0.6
	Bottom	–1.66	–1.69	–1.7	–1.71	–1.65	–1.71
Total residual stresses (MPa)	Top	–19.51	–18.35	–18.96	–18.87	–18.75	–18.85
	Middle	8.64	8.66	8.71	7.8	7.75	7.78
	Bottom	–19.75	–17.12	–1.7	–19.02	–16.19	–17.38

Top ($z=3$ mm), middle ($z=1.5$ mm) and bottom ($z=0$ mm)

Table 5 Maximum deflection of the plates obtained through experimental measurements and simulations for different packing pressures

	25–25 °C			25–40 °C		
	80%	100%	120%	80%	100%	120%
Experimental [mm]	0.320	0.285	0.266	0.606	0.379	0.577
Simulation [mm]	0.329	0.298	0.278	0.565	0.396	0.589
% error	-2.81	-4.56	-4.51	6.77	-4.49	-2.08

(25–40 °C) cooling, both with the crystallization module coupled. Figure 6 shows the residual stress distribution across the plate thickness at a distance $L = 47$ mm. The results are summarized in Table 4. Stresses are compressive in the outer layers and tensile in the inner ones.

Pressure-induced residual stresses show significant variations with varying packing pressure near the mold walls, for thicknesses lower than 0.5 mm and higher than 2.5 mm. When a packing pressure of 80% of the injection pressure is used for both cooling cases, maximum compressive stresses are found at the surface of the plate. However, when packing pressure is increased, the maximum compressive stresses are found 0.2 mm inside the plate ($z = 0.2$ mm and $z = 2.8$ mm). At the core layers, tensile stresses slightly increase with packing pressure. Although the packing pressure is not applied near the layers at the core, the variation is due to the average formation pressure, P_f , which was obtained across the thickness of the plate. In general terms, pressure-induced residual stresses kept the same distribution (compressive-tensile-compressive) for packing pressures equal to 80, 100 and 120% of the injection pressure.

As observed in Table 5, for the 25–25 °C cooling case, increasing the packing pressure decreases the maximum deflection of the plate for both simulated and experimental data. This is explained by the higher pressure that pushes the polymer against the mold walls, compensating for the thermal contraction during cooling. For the 25–40 °C cooling case, behavior is different. When the packing pressure is equal to the injection pressure (100%), maximum deflection decreases from 0.564 mm (80%) to 0.396 mm, however, when it is increased to 120%, deflection increases to 0.589 mm.

Huang [21] studied the effects of different injection molding parameters on the deformation of the molded part. He analyzed packing pressure, mold temperature, injection temperature, filling time and packing time. The results showed that packing pressure and injection and mold temperature are the more significant factors in the part deformation. In addition, it was reported that for packing pressures lower than 85% of the injection pressure, deformation decreases as pressure increases, reaching the lowest value of deformation at 85%. Afterward, an increase in packing pressure increases deformation. This was explained by the excessive packing of the polymer inside the cavity, generating very high compressive stresses that, when the part is ejected, relax, generating a higher deformation. This effect was observed for the 25–40 °C cooling case: first a decrease and then an increase in deformation as packing pressure increases.

Comparing experimental results with the maximum deflection values obtained in the simulations, errors of -2.81 , -4.56 and -4.51% were found for the symmetrical cooling case and packing pressures of 80, 100 and 120%, respectively. For the 25 – 40°C cooling condition, errors of 6.77 , -4.49 and -2.08% were found for packing pressures of 80, 100 and 120%, respectively. This shows good agreement between experimental results and the simulations performed using the residual temperature and pressure fields concepts in 2D while including a crystallinity model with different packing pressures.

Conclusions

In this study, the effect of considering crystallization kinetics in the prediction of thermal and pressure-induced residual stresses was investigated. It was found that crystallization generated a temperature plateau, observed in the thermal history plots of the polymer, due to the evolution of latent heat (heat source on the balance equation). This plateau was more evident at the core layers and appeared at temperatures close to the melting point and at times when crystallization started as shown in the evolution of absolute crystallinity plots. It was found that considering crystallization in the prediction of residual stresses decreased the % error between predicted deflection and experimental results, from 0.52 – 7.34 to 3.0 – 56.3% for the symmetrical and asymmetrical cooling cases. In all cases a similar distribution of total residual stresses was found: compressive at the surfaces and tensile at the core.

The effect of varying the packing pressure was also investigated. Packing pressures of 80, 100 and 120% of the injection pressure were used in the simulations. It was found that increasing the packing pressure, up to certain value, decreased the deflection of the molded part. However, increasing it further resulted in an increase in deflection. This is due to the excessive packing of the polymer inside the cavity that causes excessive relaxation when the part is ejected. Simulation results were compared with experimental data errors between -2.08 and 6.77% were found for the analyzed cooling conditions. This shows good agreement between experimental results and the simulations performed using the residual temperature and pressure fields concepts in 2D while including a kinetic model of crystallization with different packing pressures.

Acknowledgements The authors would like to gratefully acknowledge the financial support from the Mexican National Council for Science and Technology (CONACyT).

Author contribution ME-G: Investigation, other contributions. UF-L: Conceptualization, Methodology, Supervision, Formal Analysis. AG-M: Conceptualization, Methodology, Supervision, Formal Analysis, Writing–Review and Editing. RAG-L: Formal Analysis, Writing Original draft and Editing.

Declarations

Conflict of Interest The authors declare that they have no conflicts of interest to this work.

References

1. Thakkar BS, Broutman LJ (1980) The influence of residual stresses and orientation on the properties of amorphous polymers. *Polym Eng Sci* 20(18):1214–1219
2. Chaoui K, Chudnovsky A, Moet A (1987) Effect of residual stress on crack propagation in MDPE pipes. *J Mater Sci* 22:3873–3879
3. Hornberger LE, Devries KL (1987) The effect of residual stress on the mechanical properties of glassy polymers. *Polym Eng Sci* 27(19):1473–1478
4. Guevara-Morales A, Figueroa-López U (2014) Residual stresses in injection molded products. *J Mater Sci* 49:4399–4415
5. Baaijens FPT (1991) Calculation of residual stresses in injection molded products (in English). *Rheola Acta* 30(3):284–299. <https://doi.org/10.1007/BF00366642>
6. Daly HB, Nguyen K, Sanschagrín B, Cole K (1998) Build-up and measurement of molecular orientation, crystalline morphology, and residual stresses in injection molded parts: a review. *J Inject Molding Technol (USA)* 2(2):59–85
7. Isayev AI, Crouthamel DL (1984) Residual stress development in the injection molding of polymers. *Polymer-Plastics Technol Eng* 22(2):177–232. <https://doi.org/10.1080/03602558408070038>
8. Kamal MR, Lai-Fook RA, Hernandez-Aguilar JR (2002) Residual thermal stresses in injection moldings of thermoplastics: a theoretical and experimental study. *Polym Eng Sci* 42(5):1098–1114. <https://doi.org/10.1002/pen.11015>
9. Jansen KMB, Pantani R, Titomanlio G (1998) As-molded shrinkage measurements on polystyrene injection molded products. *Polym Eng Sci* 38(2):254–264. <https://doi.org/10.1002/pen.10186>
10. Jansen KMB, Van Dijk DJ, Freriksen MJA (1998) Shrinkage anisotropy in fiber reinforced injection molded products. *Polym Compos* 19(4):325–334. <https://doi.org/10.1002/pc.10105>
11. Wagner J, Phillips PJ (2001) The mechanism of crystallization of linear polyethylene, and its copolymers with octene, over a wide range of supercoolings. *Polymer*. 42(21):8999–9013
12. Phillips R, Manson JE (1997) Prediction and analysis of nonisothermal crystallization of polymers. *J Polym Sci Part B: Polym Phys* 35(6):875–888
13. Tropsa V, Ivankovic A, Williams JG (2000) Predicting residual stresses due to solidification in cast plastic plates. *Plast, Rubber Compos* 29(9):468–474
14. Tropsa V (2001) Predicting residual stresses due to solidification in cast plastic plates, PhD, Mechanical Engineering Department, Imperial College of Science, Technology and Medicine, London, UK
15. Jansen K (1994) Residual stresses in quenched and injection moulded products. *Int Polym Proc* 9(1):82–89
16. Estrella-Guayasamin M, Figueroa-López U, Guevara-Morales A (2019) Prediction of residual stresses in injection-molded plates using the residual temperature field concept. *Polym Eng Sci* 59(11):2220–2230. <https://doi.org/10.1002/pen.25225>
17. Zhang X, Fujii M (2003) Measurements of the thermal conductivity and thermal diffusivity of polymers. *Polym Eng Sci* 43(11):1755–1764
18. Choe CR, Lee KH (1989) Nonisothermal crystallization kinetics of poly (etheretherketone) (PEEK). *Polym Eng Sci* 29(12):801–805
19. Tobin MC (1974) Theory of phase transition kinetics with growth site impingement. I. homogeneous nucleation. *J Polym Sci* 12:399–406
20. Zoetelief WF, Douven LFA, Ingen Housz AJ (1996) Residual thermal stresses in injection molded products. *Polym Eng Sci* 36(14):1886–1896
21. Huang M-C, Tai C-C (2001) The effective factors in the warpage problem of an injection-molded part with a thin shell feature. *J Mater Process Technol* 110(1):1–9. [https://doi.org/10.1016/S0924-0136\(00\)00649-X](https://doi.org/10.1016/S0924-0136(00)00649-X)

Publisher's Note Springer Nature remains neutral with regard to jurisdictional claims in published maps and institutional affiliations.